IEEE Access
Multidisciplinary | Rapid Review | Open Access Journal

Received April 13, 2019, accepted May 9, 2019, date of publication May 14, 2019, date of current version May 28, 2019.

Digital Object Identifier 10.1109/ACCESS.2019.2916681

Generalized Dynamics of Stacked Tensegrity Manipulators

DENIS FADEYEV, ALTAY ZHAKATAYEV, (Member, IEEE), ASKAT KUZDEUOV, AND HUSEYIN ATAKAN VAROL, (Senior Member, IEEE)
Department of Robotics and Mechatronics, Nazarbayev University, Z05H0P9 Astana, Kazakhstan

Corresponding author: Huseyin Atakan Varol (ahvarol@nu.edu.kz)

This work was partially supported by the Ministry of Education and Science of the Republic of Kazakhstan grant "Methods for Safe Human Robot Interaction with Variable Impedance Actuated Robots."

ABSTRACT Tensegrity structures emerged initially as an art form, have recently gained substantial interest among engineering researchers. The distinctive attribute of these structures is using pretensioned tensile elements connected to rigid bars to establish an equilibrium of the whole structure. Thanks to these elements, tensegrity structures are lightweight and yet robust. The main challenge impeding their widespread use is the intricate constrained nonlinear dynamics caused by the tensegrity topology. In this paper, we extend the dynamics of tensegrities by adding damping forces and incorporating forces along the connected strings passing through several nodes. As an experimental platform, a two-stage stacked tensegrity manipulator was constructed. The system was actuated using six actuators and the kinematic information of the system was acquired by measuring the node coordinates using optical motion capture. Afterward, we compared the structure behavior to the simulated one using our dynamics formulation. The results of these experiments show that our dynamics formulation is capable of representing the rich nonlinear dynamics of stacked tensegrity manipulators effectively.

INDEX TERMS Tensegrity, manipulator dynamics, robots, simulation.

I. INTRODUCTION

Tensegrity is a term derived from the conjunction of two words: *tension* and *integrity*. It was first introduced by the architect Buckminster Fuller [1]. The tensegrity structure is a combination of rigid bodies and strings (i.e. prestressed tensile elements), where the tensile elements are always in tension and rigid bodies have the ability to resist the force in both directions.

The tensegrity configuration is defined as a set of positions and orientations of the rigid bodies in a tensegrity, which can be stabilized by a specific connectivity of strings in the absence of external forces [1]. Tensegrity structures can be categorized according to their class as class-k, where k represents the maximum number of rigid elements that are in contact with each other. For example, rigid elements of class-1 tensegrity structures have no contact with each other and are connected only through tensile elements (see Fig. 1a), whereas class-2 structures have at most two bars connected to each other (see Fig. 1b).

The associate editor coordinating the review of this manuscript and approving it for publication was Dominik Strzalka.

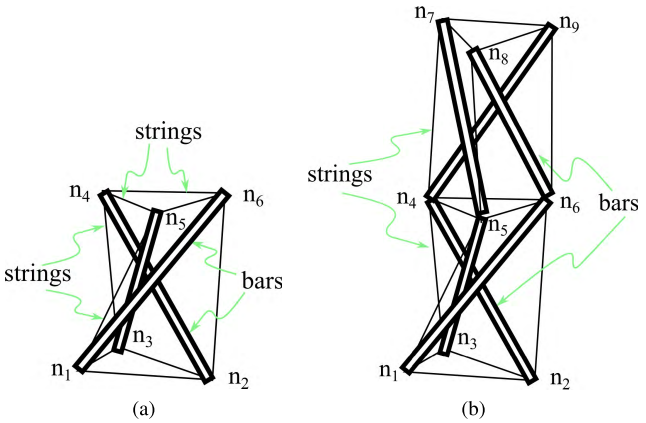

FIGURE 1. Schematics of three-dimensional tensegrity structures.

A point in 3D space where rigid and/or tensile elements of a tensegrity are connected is called a *node*. Traditionally, every connection at a node is modeled as a ball joint. Therefore, string forces acting on the rigid elements of tensegrity, in theory, generate only axial load without any moments or

shear forces. In reality, the moments and shear forces are minimal and thus, can be disregarded. This is one of the main advantages of tensegrity structures, since it leads to the known direction of every internal force in the structure. The other advantage of tensegrities is their high load-to-weight ratio thanks to the presence of prestressed tensile elements. Tensile elements are lighter than rigid bodies and their prestress makes the system more robust to external disturbances [1]. Another advantages of tensegrity structures include easy scalability and energy efficiency.

Early tensegrity structures were built as an art form with architectural grace [1]. Most early research was dedicated to equilibrium and stability analysis of tensegrities. For example, the necessary condition for stability of free-standing (i.e. without any external support) tensegrity structures was obtained using the tangent stiffness matrix [2]. Rigidity of prismatic tensegrities was analyzed using stress matrix analysis in [3]. It was shown that if the stress matrix is positive semi-definite and has the proper rank, then the associated prismatic tensegrity structure is rigid. Researchers studied the rigidity of general structures also utilizing quadratic energy forms [4]. Stiffness of prestressed structures was found by two alternative approaches: utilizing equilibrium and stress matrices [5]. This work demonstrated a link between the mathematical rigidity theory and engineering stiffness theory.

Finding stable (equilibrium) initial configuration of the tensegrity structure is called as form-finding. A form-finding method for tensegrities with multiple states of self-stress was introduced in [6]. The method only requires information about the topology and the types of members. Other examples of form-finding techniques applied for tensegrities include: Monte-Carlo method suitable for arbitrary initial configurations and large scale complex tensegrity structures with geometric constraints [7], dynamic relaxation method applicable for tensegrities with variable topology [8], genetic algorithms for self-stressed (free-standing) [9] and regular [10] tensegrities, finite element methods tailored for statically indeterminate tensegrities [11], multi-parameter form-finding [12], and graph-based approach for complex, irregular and scalable tensegrities [13]. This list of form-finding techniques is by no means exhaustive and the reader is referred to [14], [15] for further information. The aforementioned initial research in static equilibrium conditions for tensegrity structures was driven by their potential in civil engineering.

The use of tensegrity paradigm in robotics and aerospace, however, requires the dynamics formulation of these systems. The earlier results on tensegrity dynamics were achieved by studying the force-displacement relationships, which describe how the structures move under external loads. Transfer function between an input excitation and the resulting structural oscillation was found by using the second order dynamic tensegrity model [16]. However, due to the assumption of constant matrices in the equations, the solutions were valid only for small oscillations around the equilibrium. Equilibrium and compatibility conditions were utilized to investigate the behavior of tensegrity structures under small perturbations around the equilibrium [17]. Exact analytical solution for the force-displacement relationship of a simple tensegrity was found by using the minimum energy condition in terms of the nodal configuration and edge stresses [18]. Shape control of a tensegrity structure by adjusting the bar lengths was considered in [19]. Researchers employed Newtonian formulation to develop non-linear tensegrity model using constrained particle dynamics subject to the principle of virtual work.

Full nonlinear dynamics of class-1 tensegrities was derived in [20]. The work used Lagrangian methodology to formulate the equations in vector second order form with independent generalized coordinates. Due to the system topology, the approach yields highly nonlinear terms with transcendental functions, which results in a complicated mathematical representation. Linearized dynamic equations were derived based on both Eulerian and Lagrangian formulations [21], [22]. Based on these equations, harmonic analysis of a three-bar tensegrity and of a six-stage tensegrity prism were performed. However, the obtained equations were valid only around the neighborhood of a reference configuration, around which the system was linearized. Modal analysis of icosahedral and dodecahedral tensegrities was performed in [23]. It was shown that natural frequencies of infinitesimal mechanism modes increase as the square root of the amplitude of the prestress. A comprehensive summary of tensegrity dynamics can be found in [24].

Several works have focused on the control of tensegrity structures. For example, a method to determine the tendon force inputs that will move the tensegrity structure from one configuration into another along a predefined path was tackled in [25]. The method was based on feedback linearization that utilizes the parameters in the null space of control distribution matrix to obtain admissible and non-saturating inputs. Dynamics of tensegrity structures was utilized also for their locomotion [26]. Specifically, two tensegrity robots were considered: triangular tensegrity prism with three bars and quadrilateral tensegrity prism with four bars. For each of these robots, automatic controllers based on evolutionary algorithms were developed in order to simulate their locomotion based on periodic gate. It was shown that the locomotion ability of tensegrity robots does not drastically decrease in case of a single actuator failure. Vibration control of a three-stage tensegrity tower using active damping was presented in [27]. Integral force feedback, acceleration feedback control and active control methods were evaluated by their ability to reduce the acceleration transmissibility from the bottom base to the top plate. It was shown that force and acceleration feedback control can effectively suppress the first two bending modes of the tensegrity tower. The active feedback control [28] was used to adjust the natural frequencies of the tensegrities by changing the string stresses. The authors demonstrated the effectiveness of the vibration control of the five-module tensegrity obtained by shifting the natural frequencies of the system.

In order to simplify the complexity of formulation with independent generalized coordinates, the nonminimal coordinates representation of tensegrity dynamics was introduced in [29]–[31]. In this formulation the system was described with directional vectors of the rigid elements and the positions of their centers. The formulation leads to a larger state space, yet there are several advantages of this formulation. Firstly, it eliminates all transcendental functions from the equations. Secondly, the mass-inertia matrix does not depend on the system states. Therefore, its inverse needs to be computed only once and can be used at all subsequent iterations of simulation. Later work [32] has transformed this dynamics describing the system as 3D positions of the nodes and imposing nodal constraints to preserve the constant length of rigid elements. One of the advantages of this formulation is that it can be easily extended to higher class tensegrity structures by adding virtual nodes while preserving the pairwise connection of the bars to the nodes. We note that alternative equations of motion of the tensegrities might be obtained by Kane's approach [33], Gibbs-Appell formulation [34] or Udwadia-Kalaba equations [35]. These methods were specifically devised for constrained (holonomic or nonholonomic) and multibody systems.

All of the above formulations of tensegrity dynamics did not include the damping effects, contrary to the real-world tensegrity structures. With the old formulations, a prestressed tensegrity structure, initially at an equilibrium configuration, would start to oscillate if an external impulsive force is applied to one or more of its nodes. These oscillations would be long-lasting. In reality, the oscillations die out rather quickly, which indicates that the damping effects are significant. As the complexity and size of tensegrity structures increase, the discrepancy between their undamped simulations and their real-world damped behavior is expected to increase. Additionally, simulation of deployable tensegrity structures and investigation of their utilization as vibration isolators demand incorporation of dissipative forces into their dynamics equations. Recently, damping forces were incorporated into dynamics of tensegrity bridges [36]. However, the paper contains only simulation results, there is no experimental verification of this damped dynamics of tensegrities, and the structure is not actuated.

In tensegrity structures considered up to date, a single string connects only two nodes. In order to obtain a fully controllable tensegrity robot, each strings needs to be actuated by an individual actuator. Therefore, for complex and large tensegrity systems, number of strings and of the corresponding actuators, increases rapidly. From the control perspective, this is challenging and undesirable. High number of actuators will increase the energy consumption and mass of the tensegrity robots, thus ultimately diminishing and blurring their advantages. One solution to this problem is to make a single actuator control several strings. Therefore a single string, which connects multiple nodes, needs to be implemented in the tensegrity structure. This way it is possible to reduce number of necessary actuators and to place them as close to the base as possible and decrease the overall moment of inertia and mass of the system. Such structures would have considerable benefits for industrial applications, since most of the energy would be spent on moving the target object (end effector) rather than the robot itself, as it happens in traditional industrial manipulators. Moreover, a single string connecting multiple nodes requires less number of clamping elements, which in turn simplifies the tensegrity construction.

The contribution of this paper is twofold: Firstly, tensegrity dynamics with damping forces was formulated and the performed simulations were verified experimentally. These damping effects were incorporated into strings, which generate dissipative forces proportional to the change in the length of the strings. Secondly, cases with a single string connecting multiple nodes were incorporated into tensegrity dynamics. Several strings can be controlled by a single actuator using a single string connecting multiple nodes. In order to test the formulated tensegrity dynamics, a tensegrity structure consisting of two stages (i.e. the stacked tensegrity manipulator) was constructed. Six actuators were utilized to actuate the tensegrity by pulling and releasing the strings. An optical motion capture system consisting of eight cameras was built to measure the motion of the tensegrity robot during the experiments. Finally, simulation results were compared with real-world experimental measurements. Results showed that the proposed tensegrity dynamics formulation accurately describes the real-world tensegrity structure behavior.

The rest of the paper is organized as follows. Section II-A reviews the tensegrity dynamics as formulated in [32]. In Section II-B tensegrity dynamics with single string connecting multiple nodes is formulated, which is followed by incorporation of damping forces in Section II-C. Later the constructed tensegrity structure, which serves as the experimental platform, is described in Section III. This section also includes the description of the simulations and experiments. It is followed by the presentation and discussion of the simulation and experimental results in Section IV, and the paper is finally concluded in Section V.

II. DYNAMICS OF TENSEGRITY STRUCTURES

A. CONSTRAINED DYNAMICS OF TENSEGRITY STRUCTURES

In this section, we adopt the derivation of the constrained tensegrity dynamics from [32]. The description of the notations used in this section can be found in Table 1.

Each point, where rigid and tensile elements are connected, is called a physical node $n_i, i \in \{1, \ldots, \mu\}$, where μ is the total number of physical nodes. The rigid elements (i.e. bars) are denoted with $b_i, i \in \{1, \ldots, \beta\}$ where β is the total number of rigid elements and b_i is the directional vector of i-th bar, Fig. 2. Similarly, tensile elements are represented with $s_i, i \in \{1, \ldots, \sigma\}$, where σ is the total number of tensile elements and s_i is the directional vector of i-th string. Since in class-1 tensegrity structures rigid bodies are separated from each other, each node has exactly one tip of a rigid element

TABLE 1. List of the notations used in Section II-A and their descriptions.

Sym.	Dim.	Description	Alternative expression
μ	Scalar	Total number of physical nodes	
ν	Scalar	Total number of virtual nodes	
β	Scalar	Total number of bars	$(\mu+\nu)/2$
σ	Scalar	Total number of strings	
ϕ	Scalar	Total number of constraints	
n_i	$\mathbb{R}^3$	3D position of i-th physical node	$[n_{ix}\ n_{iy}\ n_{iz}]^T$
n'_i	$\Re^3$	3D position of i-th virtual node	$[n'_{ix}\ n'_{iy}\ n'_{iz}]^T$
b_i	$\Re^3$	3D directional vector of i-th bar	$[b_{ix}\ b_{iy}\ b_{iz}]^T$
s_i	$\Re^3$	3D directional vector of i-th string	$[s_{ix}\ s_{iy}\ s_{iz}]^T$
N	$\Re^{3\times 2\beta}$	Node position matrix	$[n_1\ \dots\ n_\mu\ n'_1\ \dots\ n'_\nu]$
C_b	$\Re^{\beta\times 2\beta}$	Bar connectivity matrix	
C_r	$\Re^{\beta\times 2\beta}$	Bar center connectivity matrix	$\lvert C_b\rvert$
C_s	$\Re^{\sigma\times 2\beta}$	String connectivity matrix	
B	$\Re^{3\times\beta}$	Bar direction matrix	$[b_1\ \dots\ b_\beta]=NC_b^T$
S	$\Re^{3\times\sigma}$	String direction matrix	$[s_1\ \dots\ s_\sigma]=NC_s^T$
m_i	Scalar	Mass of i-th bar	
$\hat{m}$	$\Re^{\beta\times\beta}$	Diagonal mass matrix	$\langle[m_1\ m_2\ \dots m_\beta]\rangle$
$\mathcal{M}$	$\Re^{2\beta\times 2\beta}$	Mass-inertia matrix	Equation (1)
W	$\Re^{3\times 2\beta}$	Matrix of exogenous forces	$[w_1\ w_2\ \dots\ w_\beta]$
l_i	Scalar	Length of i-th bar	$\lvert\lvert b_i\rvert\rvert$
$\hat{l}$	$\Re^{\beta\times\beta}$	Diagonal matrix of bar lengths	$\langle[l_1\ l_2\ \dots\ l_\beta]\rangle$
h_i	Scalar	Length of i-th string	$\lvert\lvert s_i\rvert\rvert$
h_i^0	Scalar	Rest length of i-th string	
κ_i	Scalar	Stiffness coefficient of i-th string	
γ_i	Scalar	Stiffness force density on i-th string	Equation (2)
$\hat{\gamma}$	$\Re^{\sigma\times\sigma}$	Diagonal stiffness force density matrix	$\langle[\gamma_1\ \gamma_2\ \dots\ \gamma_\sigma]\rangle$
t_i	$\Re^3$	Tension force vector along the i-th string	$\gamma_i s_i$
T	$\Re^{3\times\sigma}$	Matrix of tension forces along each string	$[t_1\ \dots\ t_\sigma]=S\hat{\gamma}$
F_s	$\Re^{3\times 2\beta}$	Matrix of tension forces applied at each node	$-TC_s=-NC_s^T\hat{\gamma}C_s$
P	$\Re^{2\beta\times\phi}$	Nodal constraint matrix	
Λ	$\Re^{3\times\phi}$	Constraint value matrix	
Ω	$\Re^{3\times\phi}$	Lagrangian multiplier matrix	
F_c	$\Re^{3\times 2\beta}$	Constraint force matrix	ΩP^T
$\hat{\lambda}$	$\Re^{\beta\times\beta}$	Diagonal matrix of reaction force densities	Equation (5)
$\mathcal{K}$	$\Re^{2\beta\times 2\beta}$	Matrix of nodal force densities	$C_s^T\hat{\gamma}C_s-C_b^T\hat{\lambda}C_b$

connected to it, i.e. $\mu = 2\beta$. Higher class tensegrities can also be formulated in constrained class-1 form. For this, all rigid elements are modeled as separate bars. Additional virtual nodes are introduced for the "freed" tips of these rigid elements. In total, the system should result in ν virtual nodes n'_i, $i \in \{1,\dots,\nu\}$, such that $\nu+\mu=2\beta$.

The *node position matrix* is constructed by stacking physical and virtual node vectors as columns: $N = [n_1\ \dots\ n_\mu\ n'_1\ \dots\ n'_\nu]$. By defining a constant *bar connectivity matrix* C_b, it is possible to compute the bar directional vectors b_i from the node position matrix N. Each bar connects exactly two of either physical or virtual nodes, i.e. $b_i = n_j - n_k;\ i \in \{1,\dots,\beta\};\ j,k \in \{1,\dots,2\beta \mid j \neq k\}$. Therefore, $C_b^{i,j}=1$ and $C_b^{i,k}=-1$ ($A^{i,j}$ denotes the element of i-th row and j-th column of matrix A). All other elements of C_b are zero. The *bar direction matrix* is then defined as $B=NC_b^T$, where its i-th column is the vector b_i, while superscript T denotes matrix transpose.

The *string connectivity matrix* is derived similarly. The i-th string connects exactly two of either physical and/or virtual nodes, $s_i = n_j - n_k;\ i \in \{1,\dots,\sigma\};\ j,k \in \{1,\dots,2\beta \mid j \neq k\}$. Therefore, $C_s^{i,j}=1$ and $C_s^{i,k}=-1$. All other elements of C_s are zero. The *string direction matrix* is then defined as $S=NC_s^T$, where the i-th column of S is the vector s_i.

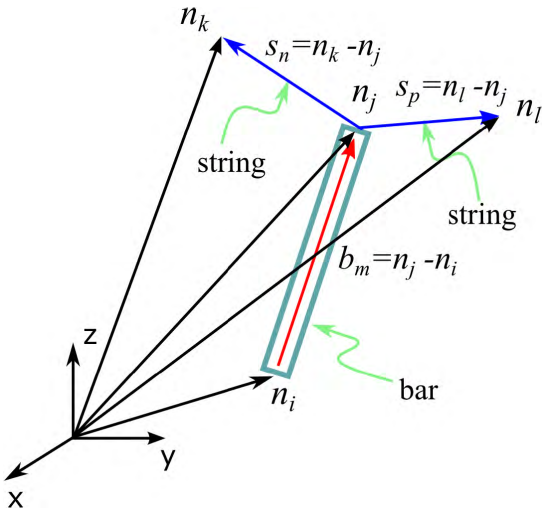

FIGURE 2. Schematic diagram of a tensegrity bar and strings.

Since strings are very light compared to the other elements of the structure, their mass is assumed to be negligible. Furthermore, the bars are assumed to have a uniform cross-section with their center of mass located exactly at the geometric center. Because of this assumption, inertia of a single bar about its long axis becomes negligible. It is further assumed that the bars have zero thickness. By using the masses of the bars, a diagonal mass matrix $\hat{m} = \langle[m_1\ m_2\ \dots m_\beta]\rangle$ can be constructed, where $\langle\cdot\rangle$ is a diagonal operator, which returns a diagonal matrix given a vector or a vector of the diagonal elements given a square matrix. The mass-inertia matrix is then defined as

$$\mathcal{M}=\frac{1}{12}(C_b^T\hat{m}C_b+3C_r^T\hat{m}C_r), \tag{1}$$

where $C_r = \lvert C_b\rvert$ ($\lvert\cdot\rvert$ represents the absolute value of all elements in the matrix).

The matrix W contains all exogenous forces acting at each node, including weights generated by masses of the bars. Since it is assumed that a bar's center of mass is located exactly at its center, the weight of the bar can be split equally to both of its nodes. Taking gravity g acting in the negative z direction, the weight value will have only z component equal to $-gm_i/2$.

The string lengths can be denoted as $h_i = \lvert\lvert s_i\rvert\rvert$ and the string rest length with h_i^0. All strings of the system are assumed to exert force only when they are in tension, i.e. when the string displacement $\Delta h_i = h_i - h_i^0 > 0$. Thus, the stiffness force density in the string i can be computed as

$$\gamma_i=\begin{cases}\kappa_i\dfrac{\Delta h_i}{h_i}, & \text{if } \Delta h_i>0\\ 0, & \text{otherwise,}\end{cases} \tag{2}$$

where κ_i is the stiffness of i-th string. The tension force vector exerted by the i-th string is $t_i = \gamma_i s_i$. It denotes the tension as a vector along the direction of the string and is always parallel to s_i when $\gamma_i \neq 0$. The matrix of string tension forces can be described with $T = [t_1\ t_2\ \dots\ t_\sigma] = [\gamma_1\ s_1\ \gamma_2\ s_2\ \dots\ \gamma_\sigma s_\sigma] = S\hat{\gamma} = NC_s^T\hat{\gamma}$, where $\hat{\gamma} = \langle[\gamma_1\ \gamma_2\ \dots\ \gamma_\sigma]\rangle$. The following equation transforms string tension forces to the nodal forces: $F_s = -TC_s$. The i-th column of F_s shows the direction and magnitude of the tension force that is exerted at the i-th node by all the strings connected to it.

Since a virtual node is created at the same position as the corresponding physical node, it has to be constrained to preserve its coincidence at all simulation time steps. In order to ensure this, a *nodal constraint matrix* P and *constraint value matrix* Λ are introduced, where ϕ is the total number of constraints. These matrices are related in the following form: $NP = \Lambda$. For instance, if we want to add the k-th constraint, which specifies that the virtual node n_i' is located at the position of physical node n_j, then the following relation should be satisfied: $n_j - n_i' = 0$. From this, it follows that $P^{j,k} = 1$, $P^{(\mu+i),k} = -1$, $\Lambda^{1:3,k} = 0$, with all other elements of the column k of P filled with zeros. The forces, which are generated by all constraints at all nodes can be written in the matrix form $F_c = \Omega P^T$, where Ω is the *Lagrangian multiplier matrix* and is computed by solving the algebraic equation (the whole solution is elegantly derived in [32])

$$N\mathcal{K}\mathcal{M}^{-1}P - \Omega P^T\mathcal{M}^{-1}P = W\mathcal{M}^{-1}P. \tag{3}$$

The overall dynamics of the system can be written as

$$\ddot{N}\mathcal{M} + N\mathcal{K} = W + F_c, \tag{4}$$

The term $N\mathcal{K}$ in (4) represents the string tension forces, together with the reaction forces along the bars, which occur due to the imposed constraints. The matrix $\mathcal{K}$ is given as $\mathcal{K} = C_s^T\hat{\gamma}C_s - C_b^T\hat{\lambda}C_b$, where $\hat{\lambda}$ is

$$\hat{\lambda} = \frac{1}{2}\langle\langle\hat{l}^{-2}B^T(TC_s - W - F_c)C_b^T - \frac{1}{6}\hat{l}^{-2}\hat{m}\dot{B}^T\dot{B}\rangle\rangle, \tag{5}$$

with $\hat{l} = \langle[l_1\, l_2\, \dots\, l_\beta]\rangle$ denoting a matrix of fixed bar lengths. Physically, $\hat{\lambda}$ is a diagonal force density matrix, with every diagonal element representing a force density acting along a corresponding bar. The force density includes bar reaction forces as well as constraint force required to preserve the bar length. The equation is derived from single bar dynamics in [29] and [32].

B. TENSEGRITY DYNAMICS WITH COMPOSITE STRINGS

This section covers the derivation of the forces produced by strings when the structure has composite strings passing through several nodes. The notations used in this and the subsequent sections are summarized in Table 2. We define a *composite string* as a string, which physically connects two or more nodes. In other words, it represents a string, which is a single physical entity and can pass through several nodes. A composite string has unique physical parameters: Young's modulus, cross-sectional area and rest length. A *simple string* will refer to a portion of composite string that connects exactly two nodes. For example, in Fig. 2 both s_n and s_p are portions of a single composite string, which passes through nodes n_l, n_j, and n_k. In order to compute the tension in both strings the length of the total composite string should be found. This can be done by dividing the composite string into smaller simple strings, which can be represented as vectors. The total length is then the sum of the magnitudes of both vectors.

Assuming a structure has σ_c composite strings, a vector $\xi^0 = [\xi_1^0\ \dots\ \xi_{\sigma_c}^0]^T$ can be introduced, which will denote the rest lengths of the composite strings. Since it is easier to analyze the system using simple strings, σ_s will denote the total number of simple strings and the vector $\xi = [\xi_1 \dots \xi_{\sigma_s}]^T$ will represent their current lengths, or the distance between the two nodes, to which each simple string is connected.

Composite connectivity matrix G maps the simple strings to the composite strings. For instance, if i-th composite string is divided into j-th and k-th simple strings, then $G^{j,i} = G^{k,i} = 1$, while other elements of column i of G are filled with zeros. Note that if all strings in the structure connect to exactly two nodes, simple strings can be ordered in a way such that $G = I_{\sigma_s}$, where I_{σ_s} is σ_s-by-σ_s identity matrix.

Previously in (2), the stiffness coefficient of the strings was considered to be constant, since string's rest length was assumed to be constant for all periods of time. However, the Hooke's law states that the force produced by a stretched string is $F = (EA/L_0)\Delta L$, where E, A, L_0 and ΔL are Young's modulus, string's cross-sectional area, string's rest length and string's change in length, respectively. Therefore, in systems where strings' initial lengths are changing, the effect of such strings should be taken into account.

The stiffness $\kappa_{ci} = E_iA_i/\xi_i^0$ of i-th composite string can be mapped to the stiffness vector of the simple strings with $\kappa_s = G\kappa_c$, where $\kappa_c = [\kappa_{c1}\ \dots\ \kappa_{c\sigma_c}]^T$. The *string displacement vector* $\Delta\xi = G(G^T\xi - \xi^0)$ represents the displacements of composite strings mapped to their corresponding simple strings. The force density acting along the i-th simple string is then defined as

$$\gamma_{si} = \begin{cases} \kappa_{si}\dfrac{\Delta\xi_i}{\xi_i}, & \text{if } \Delta\xi_i > 0 \\ 0, & \text{otherwise,} \end{cases} \tag{6}$$

where κ_{si} is the i-th element of κ_s and $\Delta\xi_i$ is the i-th element of the vector $\Delta\xi$. A new matrix of tension forces along each string is then constructed as $T_s = [\gamma_{s1}s_1\ \gamma_{s2}s_2\ \dots\ \gamma_{s\sigma}s_\sigma] = S\hat{\gamma}_s$, where $\hat{\gamma}_s = \langle[\gamma_{s1}\ \gamma_{s2}\ \dots\ \gamma_{s\sigma_s}]\rangle$.

C. INCORPORATING DAMPING FORCES TO TENSEGRITY DYNAMICS

In order to derive the damping forces in the strings, let us assume that the strings' rest lengths are not constant. For example, they can be varied by actuators that pull and/or release the strings. The dependence of the strings' rest lengths on the input may be described by $\xi^0(t) = \xi_0^0 + Yu(t)$, where ξ_0^0 is a vector of composite strings' rest lengths at

TABLE 2. List of the notations used in Sections II-B and II-C and their descriptions.

Sym.	Dim.	Description	Alternative exp.
σ_c	Scalar	Total number of composite strings	
σ_s	Scalar	Total number of simple strings	
α	Scalar	Total number of actuators	
$u(t)$	$\Re^{\alpha}$	Vector of inputs to the system	
Y	$\Re^{\sigma_c \times \alpha}$	Mapping matrix from inputs to composite strings	
G	$\Re^{\sigma_s \times \sigma_c}$	Mapping matrix from composite to simple strings	
ξ_0^0	$\Re^{\sigma_c}$	Vector of initial rest lengths of composite strings	
ξ_i^0	Scalar	Rest length of i-th composite string ($i = 1 \dots \sigma_c$)	
ξ^0	$\Re^{\sigma_c}$	Vector of comp. strings' rest lengths	$\xi_0^0 + Yu(t)$
ξ_i	Scalar	Length of i-th simple string	$\|\|s_i\|\|$
ξ	$\Re^{\sigma_s}$	Vector of lengths of simple strings	$[\xi_1 \dots \xi_{\sigma_s}]^T$
$\dot{\xi}_i$	Scalar	Rate of length change of i-th simple string	$\dot{s}_i^T s_i / \xi_i$
$\dot{\xi}$	$\Re^{\sigma_s}$	Vector of simple strings' rates of change in lengths	$[\dot{\xi}_1 \dots \dot{\xi}_{\sigma_s}]^T$
$\Delta\xi$	$\Re^{\sigma_s}$	String displacement vector	$G(G^T\xi - \xi^0)$
$\Delta\dot{\xi}$	$\Re^{\sigma_s}$	Rate of change in $\Delta\xi$	$G(G^T\dot{\xi} - \dot{\xi}^0)$
E_i	Scalar	Young's modulus of i-th composite string	
A_i	Scalar	Cross-sectional area of i-th composite string	
κ_{ci}	Scalar	Stiffness coefficient of i-th composite string	$E_i A_i / \xi_i^0$
κ_c	$\Re^{\sigma_c}$	Vector of composite strings' stiffness coefficients	$[\kappa_{c1} \dots \kappa_{c\sigma_c}]$
κ_{si}	Scalar	Stiffness coefficient of i-th simple string	
κ_s	$\Re^{\sigma_s}$	Vector of simple strings' stiffness coefficients	$G\kappa_c$
γ_{si}	Scalar	Stiffness force density on i-th simple string	Equation (6)
$\hat{\gamma_s}$	$\Re^{\sigma_s \times \sigma_s}$	Diagonal stiffness force density matrix	$\langle[\gamma_{s1}\ \gamma_{s2} \dots \gamma_{s\sigma}]\rangle$
T_s	$\Re^{3 \times \sigma_s}$	Matrix of tension forces along each simple string	$S\hat{\gamma_s}$
ζ_c	$\Re^{\sigma_c}$	Vector of composite strings' damping coefficients	$[\zeta_{c1} \dots \zeta_{c\sigma_c}]$
ζ_{si}	Scalar	Damping coefficient of i-th simple string	
ζ_s	$\Re^{\sigma_s}$	Vector of simple strings' damping coefficients	$G\zeta_c$
η_i	Scalar	Damping force density on i-th simple string	Equation (7)
$\hat{\eta}$	$\Re^{\sigma_s \times \sigma_s}$	Diagonal damping force density matrix	$\langle[\eta_1 \dots \eta_{\sigma_s}]\rangle$
D	$\Re^{3 \times \sigma_s}$	Matrix of damping forces along each simple string	$S\hat{\eta} = NC_s^T\hat{\eta}$
F_d	$\Re^{3 \times 2\beta}$	Matrix of damping forces applied at each node	$-DC_s = -NC_s^T\hat{\eta}C_s$
$\hat{\lambda}_d$	$\Re^{\beta \times \beta}$	Diagonal matrix of reaction force densities	Equation (8)
$\mathcal{K}_d$	$\Re^{2\beta \times 2\beta}$	Matrix of nodal force densities with damping	Equation (9)

the initial time step, $u(t)$ is a vector of α inputs and Y is the matrix that maps inputs to the corresponding composite strings. Therefore, the rest length of a composite string will have a derivative: $\dot{\xi}^0(t) = Y\dot{u}(t)$, given that the input $u(t)$ is differentiable at time step t. Therefore, the rate of change of composite strings' lengths is $\Delta\dot{\xi} = G(G^T\dot{\xi} - \dot{\xi}^0)$.

It should be noted that $\dot{\xi}_i \neq ||\dot{s}_i||$ since $\dot{s}_i$ includes both translational and rotational velocities, while $\dot{\xi}_i$ represents only translational velocity, or in other words the component of $\dot{s}_i$ along s_i. Therefore, $\dot{\xi}_i = \dot{s}_i^T s_i / \xi_i$, where s_i/ξ_i is the unit vector along s_i. Given a vector of composite strings' damping coefficients $\zeta_c = [\zeta_{c1} \dots \zeta_{c\sigma_c}]^T$, it can be mapped to simple strings' damping coefficient vector: $\zeta_s = G\zeta_c$. The damping force density acting on the i-th simple string is therefore

$$\eta_i = \begin{cases} \zeta_{si} \dfrac{\Delta\dot{\xi}_i}{\xi_i}, & \text{if } \Delta\xi_i > 0, \\ 0, & \text{otherwise,} \end{cases} \tag{7}$$

where ζ_{si} is the i-th element of ζ_s and $\Delta\dot{\xi}_i$ is the i-th element of $\Delta\dot{\xi}$. The damping forces are present when $\Delta\dot{\xi}_i < 0$ and disregarded only when composite string's total length reduces to the value below its rest length.

The damping force matrix containing force vectors along the simple strings can be calculated as $D = [\eta_1 s_1 \dots \eta_{\sigma_s} s_{\sigma_s}] = S\hat{\eta} = NC_s^T\hat{\eta}$, where $\hat{\eta} = \langle[\eta_1 \dots \eta_{\sigma_s}]\rangle$. The matrix of damping forces acting on each node is therefore $F_d = -DC_s$. The total force generated by strings is the sum of stiffness and damping forces. Therefore, both damping force and damping force density matrices are added to the stiffness force and stiffness force density matrices in the dynamics equations, respectively. These modifications affect the matrices $\mathcal{K}$ and $\hat{\lambda}$, and the new equations become

$$\hat{\lambda}_d = \frac{1}{2}\langle\langle \hat{l}^{-2}B^T((T_s + D)C_s - W - F_c)C_b^T - \frac{1}{6}\hat{l}^{-2}\hat{m}\dot{B}^T\dot{B}\rangle\rangle, \tag{8}$$

$$\mathcal{K}_d = C_s^T(\hat{\gamma} + \hat{\eta})C_s - C_b^T\hat{\lambda}_d C_b. \tag{9}$$

The dynamics with the incorporation of the new equations (8) and (9) becomes:

$$\ddot{N}\mathcal{M} + N\mathcal{K}_d = W + F_c, \tag{10}$$

The obtained equations of motion of a tensegrity structure are algorithmic. Algorithmic equations of motion are known for their efficiency when a system is large [37], [38]. Also there is no need to re-derive the equations of motion if tensegrity configuration is modified. It is sufficient only to update the necessary matrices (e.g. N, C_b, C_r, C_s and etc.) and the corresponding boundary conditions (constraints). Other advantages of equations (8)-(10) include absence of transcendental functions and constant inertia matrix, which does not depend on system states.

III. CASE STUDY

A. TWO-STAGE STACKED TENSEGRITY MANIPULATOR PROTOTYPE

We designed and built a tensegrity robot with two stages as an experimental platform (see Fig. 3). Each stage consists of six bars, seven composite string (equivalently represented as eighteen simple strings) and one upper triangular plate. The lower stage (*Stage 1*) was connected to the ground using three *bottom* nodes (n_1-n_3), while the three *bottom* nodes (n_{13}-n_{15}) of the upper stage (*Stage 2*) were rigidly attached to the upper triangular plate of the Stage 1 (see Fig. 3a). Upper triangular plate of each stage was modeled using three *virtual* bars (b_{13}-b_{15} for Stage 1 and b_{16}-b_{18} for Stage 2), with each

TABLE 3. String connectivity matrix for the tensegrity robot.

C_{s1}		C_{s2}		n_1	n_2	n_3	n_4	n_5	n_6	n_7	n_8	n_9	n_{10}	n_{11}	n_{12}
				n_{13}	n_{14}	n_{15}	n_{16}	n_{17}	n_{18}	n_{19}	n_{20}	n_{21}	n_{22}	n_{23}	n_{24}
s_{c1}	s_1	s_{c8}	s_{19}	1					−1						
	s_2		s_{20}						1					−1	
s_{c2}	s_3	s_{c9}	s_{21}		1		−1								
	s_4		s_{22}				1								−1
s_{c3}	s_5	s_{c10}	s_{23}			1		−1							
	s_6		s_{24}					1					−1		
s_{c4}	s_7	s_{c11}	s_{25}	1							−1				
	s_8		s_{26}								1				−1
s_{c5}	s_9	s_{c12}	s_{27}		1							−1			
	s_{10}		s_{28}									1	−1		
s_{c6}	s_{11}	s_{c13}	s_{29}			1				−1					
	s_{11}		s_{30}							1				−1	
s_{c7}	s_{13}	s_{c14}	s_{31}				1					−1			
	s_{14}		s_{32}					−1				1			
	s_{15}		s_{33}					1		−1					
	s_{16}		s_{34}						−1	1					
	s_{17}		s_{35}						1		−1				
	s_{18}		s_{36}				−1				1				

TABLE 4. Bar connectivity matrix for the tensegrity robot.

C_{b1}		n_1	n_2	n_3	n_4	n_5	n_6	n_7	n_8	n_9	n_{10}	n_{11}	n_{12}	n'_1	n'_2	n'_3	n'_4	n'_5	n'_6
	C_{b2}	n_{13}	n_{14}	n_{15}	n_{16}	n_{17}	n_{18}	n_{19}	n_{20}	n_{21}	n_{22}	n_{23}	n_{24}	n'_7	n'_8	n'_9	n'_{10}	n'_{11}	n'_{12}
b_1	b_7	1			−1														
b_2	b_8		1			−1													
b_3	b_9			1			−1												
b_4	b_{10}							1			−1								
b_5	b_{11}								1			−1							
b_6	b_{12}									1			−1						
b_{13}	b_{16}													1	−1				
b_{14}	b_{17}															1	−1		
b_{15}	b_{18}																	1	−1

TABLE 5. Composite string rest lengths, stiffness per unit rest length, and damping coefficients.

i	1	2	3	4	5	6	7	8	9	10	11	12	13	14
ξ^0_{0i} (m)	1.49	1.5	1.53	1.46	1.51	1.5	2.16	0.8	0.76	0.75	0.78	0.77	0.77	1.18
E_iA_i (kN)	140	140	140	20	20	20	140	140	140	140	20	20	20	140
ζ_{ci} (kNs/m)	20	20	20	20	20	20	20	20	20	20	20	20	20	20

bar representing an edge of the triangle. This results in a class-3 tensegrity structure since there are at most three bars connected to each of the triangular plate's nodes (e.g. n_{10} has b_4 and two virtual bars b_{13} and b_{15} connected to it). The total mass of the plate was divided equally among the three virtual bars representing it.

We further classify the composite strings as *vertical* (*actuated* and *non-actuated*) and *saddle*. Vertical strings connect a *bottom* node (n_1-n_3 or n_{13}-n_{15}) in each stage with a corresponding *top* node (n_{10}-n_{12} or n_{22}-n_{24}) and pass through one of the *saddle* nodes (n_4-n_9 or n_{16}-n_{21}). The connectivities of strings and bars in Stages 1 and 2 are summarized in Tables 3, 4. Each actuated vertical string (s_{c1}-s_{c3} or s_{c8}-s_{c10}) is connected to a separate actuator and each non-actuated vertical string (s_{c4}-s_{c6} or s_{c11}-s_{c13}) is attached to a linear extension spring. These prestressed springs were added in series to the non-actuated strings in order to reduce their stiffness coefficient and allow strings to remain under tension for large displacements. The parameters of each string (EA, ζ and ξ^0_0) are given in the Table 5. Saddle strings (s_{c7} and s_{c14}) pass through all saddle nodes and connect all six bars in each stage.

The bars were made out of hollow aluminum tubes (m_i = 0.29 g, l_i = 0.95 m, $i = \{1, \ldots, 6\}$, 20 mm outer and 16 mm inner diameters for Stage 1, and m_i = 0.11 g, l_i = 0.5 m, $i = \{7, \ldots, 12\}$, 15 mm outer and 11 mm inner diameter for Stage 2). The bottom three nodes of Stage 1 formed an equilateral triangle with the circumscribed circle radius of 0.26 m. The top nodes were connected to the nodes of the upper plate and also formed an equilateral triangle with

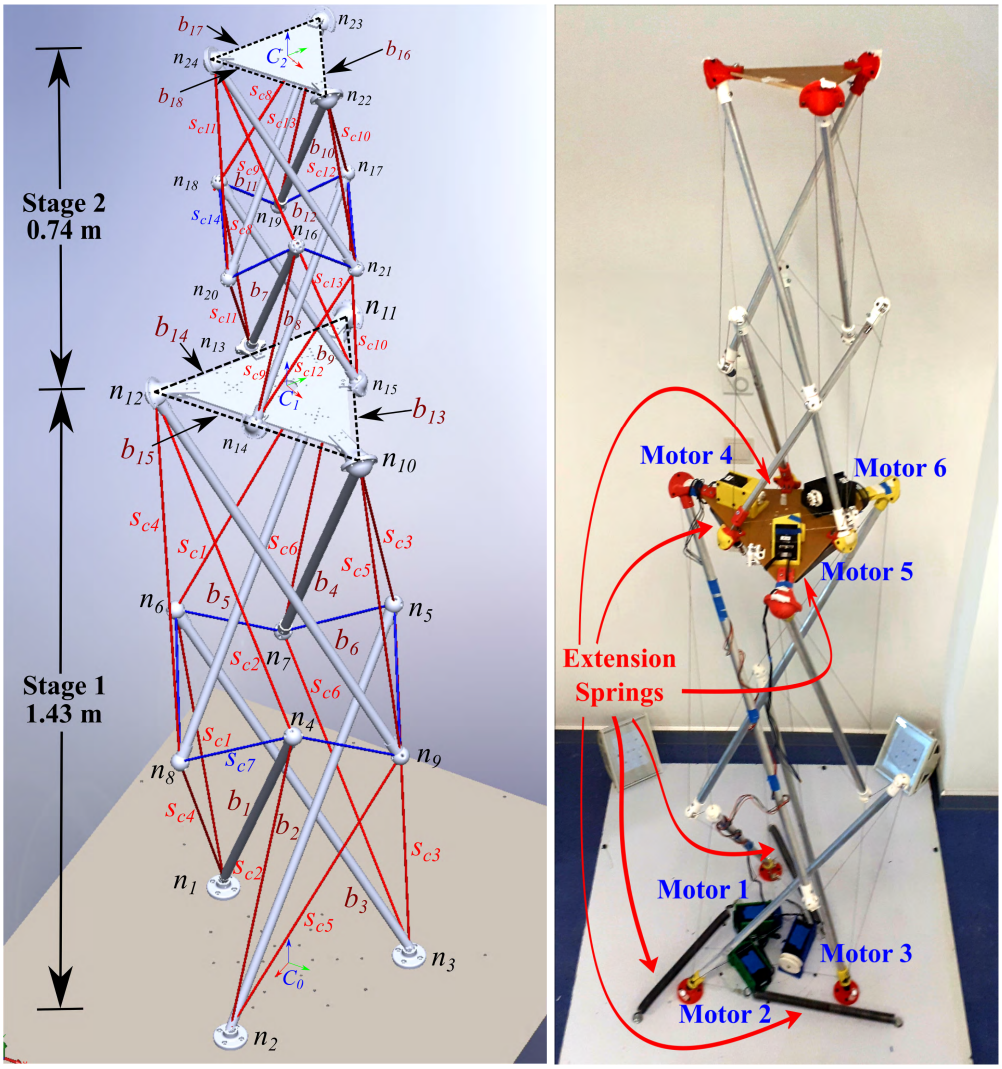

(a) (b)

FIGURE 3. Two-stage stacked tensegrity manipulator.

the circumscribed circle radius of 0.26 m. The total mass of top plate of Stage 1, which houses three Dynamixel Pro M42-10-S260-R actuators (0.27 kg each) and extension springs of Stage 2, is 2.7 kg. The equilateral triangle formed by bottom nodes of Stage 2 has a circumscribed circle radius of 0.13 m. The top nodes of Stage 2 were connected to the nodes of the top plate and also resulted in an equilateral triangle with the circumscribed circle radius of 0.13 m. The total mass of the top plate of Stage 2 is 0.33 kg.

B. SIMULATION OF THE TENSEGRITY STRUCTURE

Seven composite strings for each stage were represented as eighteen simple strings. In order to represent the structure in class-1 form, two virtual nodes were added for each node n_{10}-n_{12} and n_{22}-n_{24}. In total $\phi = 18$ constraints were added. The first three constraints were imposed on the bottom nodes of Stage 1, which are attached to the ground, so that they preserve their positions during the simulation. Six coincidence constraints on the virtual nodes of each stage were imposed (two for every physical node). The last three constraints deal with the connection of Stage 2 to Stage 1. Since bottom nodes of Stage 2 (n_{13}-n_{15}) are rigidly attached to the upper plate of Stage 1, they have to preserve their positions with respect to Stage 1 upper plate. Each bottom node of Stage 2 was located exactly between two corresponding nodes of the upper plate of Stage 1. Therefore, the following conditions have to be satisfied at all simulation times:

$$n_{13} = (n_{11} + n_{12})/2, \quad n_{14} = (n_{10} + n_{12})/2, \tag{11}$$

$$n_{15} = (n_{10} + n_{11})/2 \tag{12}$$

The detailed list of constraints is provided in Table 6. The simulation parameters of the stacked tensegrity manipulator prototype are as follows:

$$\mu = 24, \nu = 12, \beta = 18, \sigma_c = 14, \sigma_s = 36, \phi = 18, \alpha = 6.$$

TABLE 6. List of nodal constraints.

#	Constraint
1	$n_1 = [-0.117,\ -0.2,\ 0]^T$
2	$n_2 = [0.236,\ 0,\ 0]^T$
3	$n_3 = [-0.126,\ 0.2,\ 0]^T$
4	$n_{10} - n_1' = 0$
5	$n_{11} - n_2' = 0$
6	$n_{11} - n_3' = 0$
7	$n_{12} - n_4' = 0$
8	$n_{12} - n_5' = 0$
9	$n_{10} - n_6' = 0$
10	$n_{22} - n_7' = 0$
11	$n_{23} - n_8' = 0$
12	$n_{23} - n_9' = 0$
13	$n_{24} - n_{10}' = 0$
14	$n_{24} - n_{11}' = 0$
15	$n_{22} - n_{12}' = 0$
16	$n_{11} + n_{12} - 2n_{13} = 0$
17	$n_{10} + n_{12} - 2n_{14} = 0$
18	$n_{10} + n_{11} - 2n_{15} = 0$

The simulation of the tensegrity motion was performed on a workstation (Intel Xeon E5-2620 v4 2.1 GHz) with MATLAB 2018a using ode45 solver, which uses explicit Runge-Kutta integrator of 4th and 5th order, with absolute and relative tolerances set to 10^{-4}. Equation (10) should be transformed to a first order differential form for using the solver. In order to accomplish this, the second order dynamics is transformed into the following form

$$\ddot{N} = (W + F_c)\mathcal{M}^{-1} - N\mathcal{K}_d\mathcal{M}^{-1}, \tag{13}$$

Subsequently, introducing the state matrix of the system as $X = [N\ \dot{N}]$, the dynamics can be rewritten as: $\dot{X} = XZ + V$, where Z and V are matrices defined as

$$Z = \begin{bmatrix} 0 & -\mathcal{K}_d\mathcal{M}^{-1} \\ I & 0 \end{bmatrix}, \tag{14}$$

$$V = \begin{bmatrix} 0^T & (W + F_c)\mathcal{M}^{-1} \end{bmatrix}. \tag{15}$$

Experimental Cartesian coordinates of the nodes at the starting time were taken as the initial conditions of the nodes in simulation. Also initial pre-stress levels of the strings were computed from the equilibrium condition of the initial experimental tensegrity configuration.

C. REAL-WORLD EXPERIMENTS

Each stage was actuated with three motors located at their bottom part (Dynamixel Pro L54-50-S290-R for Stage 1 and Dynamixel Pro M42-10-S260-R for Stage 2). All motors were controlled in the position-control mode. The three actuators of each stage were provided with phase-shifted sinusoidal reference trajectories ($2\pi/3$, 0 and $-2\pi/3$ rad phase shift). The period of the input was 7 s and the amplitudes of string displacements were 36.3 mm and 16.8 mm for Stage 1 and Stage 2, respectively. The reference trajectories were sent to the motors and the motor angular positions were acquired at 80 Hz by a workstation (Intel Core i7-4790 3.60GHz CPU, Ubuntu Linux 16.04) over USB2Dynamixel module.

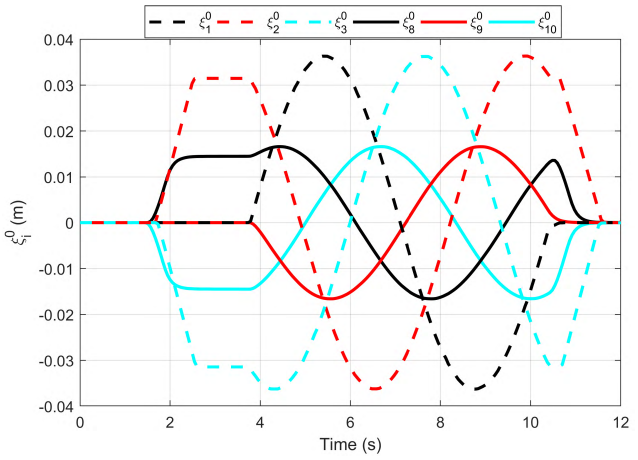

FIGURE 4. The displacements of the actuated strings.

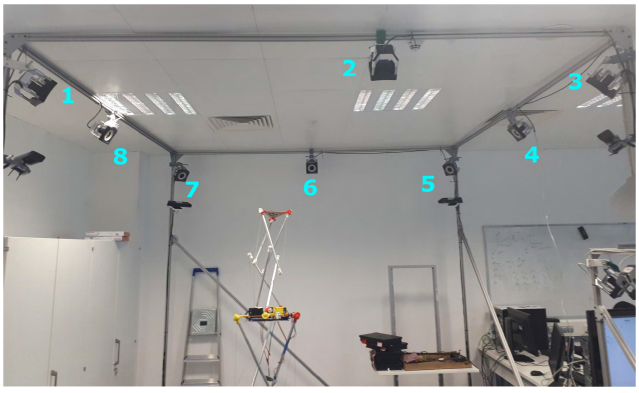

FIGURE 5. Motion capture setup to measure node coordinates in real-world experiments.

The resulting actuated string displacements are shown in the Fig. 4. In order to measure the motion of the tensegrity manipulator, a motion capture system with 3 × 3 × 3 m dimension was built using aluminum frames. The structure's motion was tracked at 120 Hz using a motion capture system with eight OptiTrack Prime 41 cameras. Spherical infrared reflective markers (10 mm diameter) were attached to the nodes of the tensegrity robot for tracking (see Fig. 5).

IV. RESULTS AND DISCUSSION

Starting from the initial nodal positions of the real robot (shown in Table 7), two different simulations were performed by applying the same inputs as obtained from the motors (see Fig. 4). One of the simulations contained the damping force, while the other did not. We defined three reference frames to compare the trajectories performed by the real robot and the simulated robot: Ground (C_0), Stage 1 plate (C_1), and Stage 2 plate (C_2) (see Fig. 3a). All frames were positioned at the centers of their triangles, which were computed by taking the mean of triangle's edges:

- Ground: $r_0 = (n_1 + n_2 + n_3)/3$
- Stage 1 plate: $r_1 = (n_{10} + n_{11} + n_{12})/3$
- Stage 2 plate: $r_2 = (n_{22} + n_{23} + n_{24})/3$

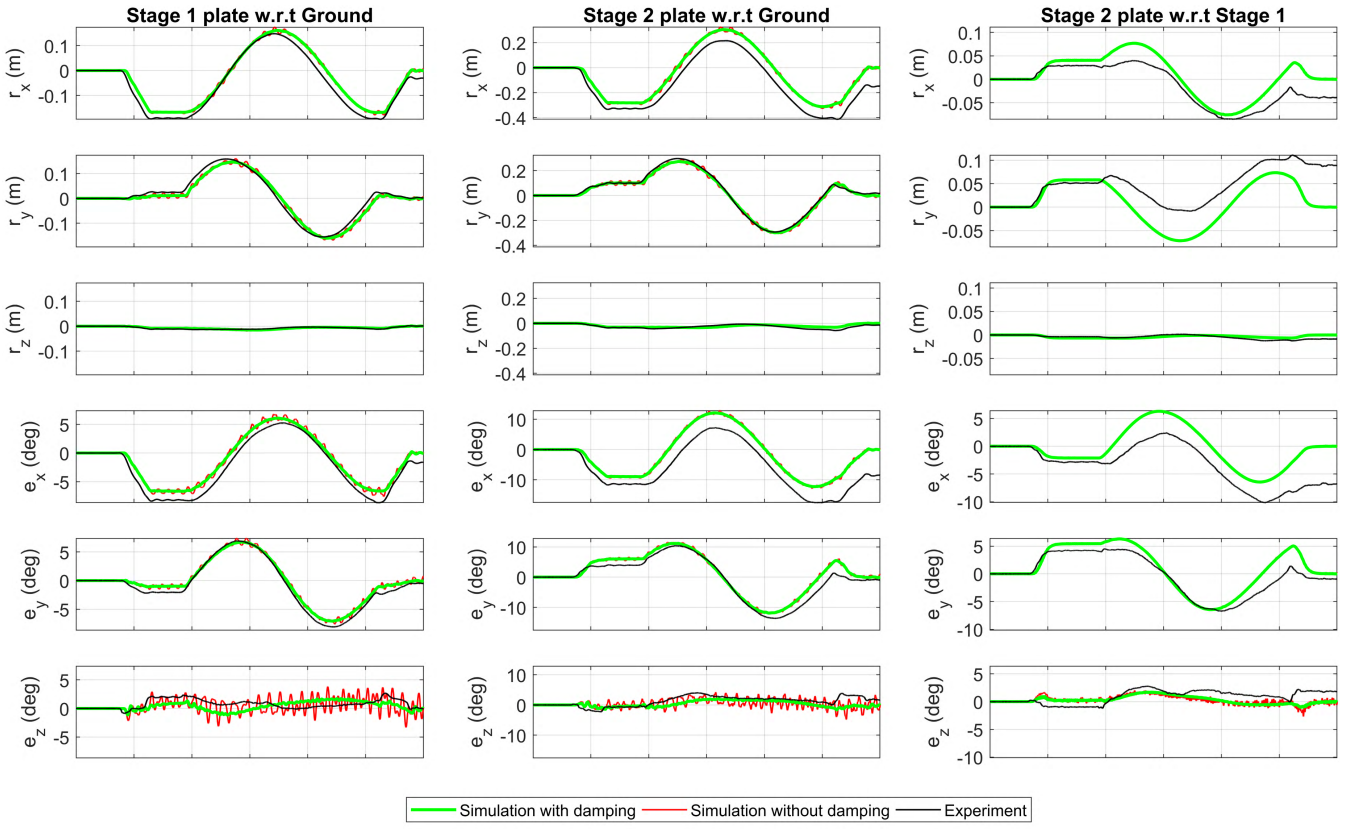

FIGURE 6. Positions and orientations of the plates obtained from the real-word experiment and computer simulations with and without damping force.

The coordinate axes of each frame were set as:

- Ground: $x_0 = \frac{(n_2 - r_0)}{||n_2 - r_0||}$, $z_0 = \frac{(n_3 - r_0) \times (n_1 - r_0)}{||(n_3 - r_0) \times (n_1 - r_0)||}$, $y_0 = z_0 \times x_0$
- Stage 1 plate: $x_1 = \frac{(n_{10} - r_1)}{||n_{10} - r_1||}$, $z_1 = \frac{(n_{12} - r_1) \times (n_{10} - r_1)}{||(n_{12} - r_1) \times (n_{10} - r_1)||}$, $y_1 = z_1 \times x_1$
- Stage 2 plate: $x_2 = \frac{(n_{22} - r_2)}{||n_{22} - r_2||}$, $z_2 = \frac{(n_{24} - r_2) \times (n_{22} - r_2)}{||(n_{24} - r_2) \times (n_{22} - r_2)||}$, $y_2 = z_2 \times x_2$

Consequently, the frames were represented in the homogeneous matrix form as:

$$C_k = \begin{bmatrix} x_k & y_k & z_k & r_k \\ 0 & 0 & 0 & 1 \end{bmatrix}, \quad \in \Re^{4\times4}, \; k \in \{0, 1, 2\}. \quad (16)$$

Three respective frames were computed for visualization:

1) Stage 1 plate with respect to Ground: ${}^0C_1 = C_0^{-1}C_1$.
2) Stage 2 plate with respect to Ground: ${}^0C_2 = C_0^{-1}C_2$.
3) Stage 2 plate with respect to Stage 1 plate: ${}^1C_2 = C_1^{-1}C_2$.

The positions of each respective frame were taken as ${}^ir_j = {}^iC_j^{1:3,4}$ and the orientations were computed by converting ${}^iC_j^{1:3,1:3}$ rotation matrix to *ZYX* Euler angles. Fig. 6 shows positions and orientation angles of ${}^0C_1$, ${}^0C_2$, and ${}^1C_2$ for the two simulations and the experiment. It can be seen from the Fig. 6 that system with no damping forces has more oscillations than the real system. Whereas the system with added damping force matches the real trajectories more closely. These results show that damping forces are present in the real system and one way to model them is to embed them as forces in the strings. Also, for the same tensegrity configuration and motor inputs additional simulation was conducted with all strings set to be connecting only two nodes. This was done to examine how the system behaves without composite strings. The trajectories do not differ very much from the previous simulation, however the discrepancy between the real trajectory is higher. The largest discrepancy was observed in the Z-axis Euler angle and it can be observed from Fig. 8. The simulated tensions on the non-actuated vertical strings are shown in Fig. 7.

As expected, discrepancy between the simulation and the experiment is larger for the second stage positions and angles. This is due to accumulation of error, i.e. discrepancy of the first stage adds to the discrepancy of the second stage. The mismatch between the simulation and the experiment might be attributed to several factors. One is the negligence of the inertia of virtual bars. As mentioned above, triangular plates of each stage were approximated by slender virtual bars. Virtual bars take into account only the mass of the plates, misrepresenting their actual inertia. Another factor might be the presence of non-negligible and nonlinear (e.g. Coulomb) sliding friction between composite strings and nodes, through which these strings pass. These frictional forces would increase the damping of the tensegrity system

TABLE 7. Initial node coordinates (mm).

	x	y	z
n_1	−117	−210	5
n_2	236	1	−4
n_3	−126	200	−2
n_4	127	24	904
n_5	−225	102	833
n_6	−110	−264	839
n_7	−267	−72	593
n_8	44	−242	545
n_9	−26	171	572
n_{10}	113	217	1426
n_{11}	−244	−15	1432
n_{12}	135	−208	1440
n_{13}	−55	−112	1436
n_{14}	124	4	1433
n_{15}	−66	101	1429
n_{16}	111	52	1878
n_{17}	−73	120	1878
n_{18}	11	−94	1883
n_{19}	−82	−15	1706
n_{20}	99	−67	1741
n_{21}	19	129	1708
n_{22}	26	178	2155
n_{23}	−127	16	2180
n_{24}	91	−36	2175

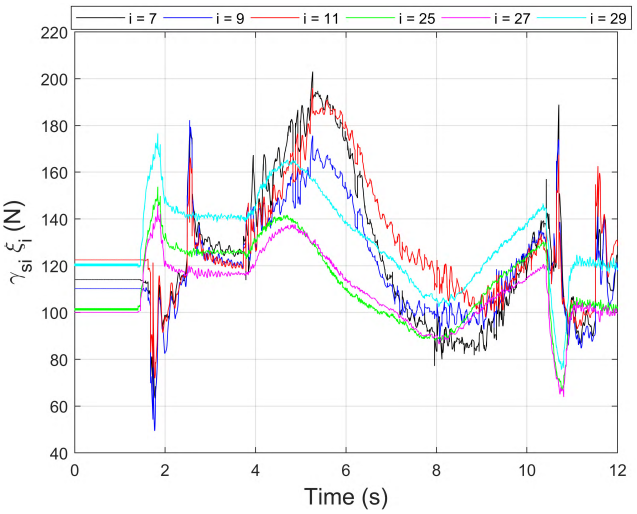

FIGURE 7. Forces on the nonactuated vertical strings.

and would reduce the amplitudes of its motion. The third source of error might be attributed to the presence of bending moments acting on the bars. These moments appear due to finite distance between holes in node attachments (through which strings pass) and bars' long axes. The root mean squared deviation of the trajectories was computed as 30.5 mm for position and 2.44 deg for orientation. The maximum value which the error in bar length preservation reached was 0.0058% of the actual bar length. The videos of the experiments are provided in the supplemental multimedia material.

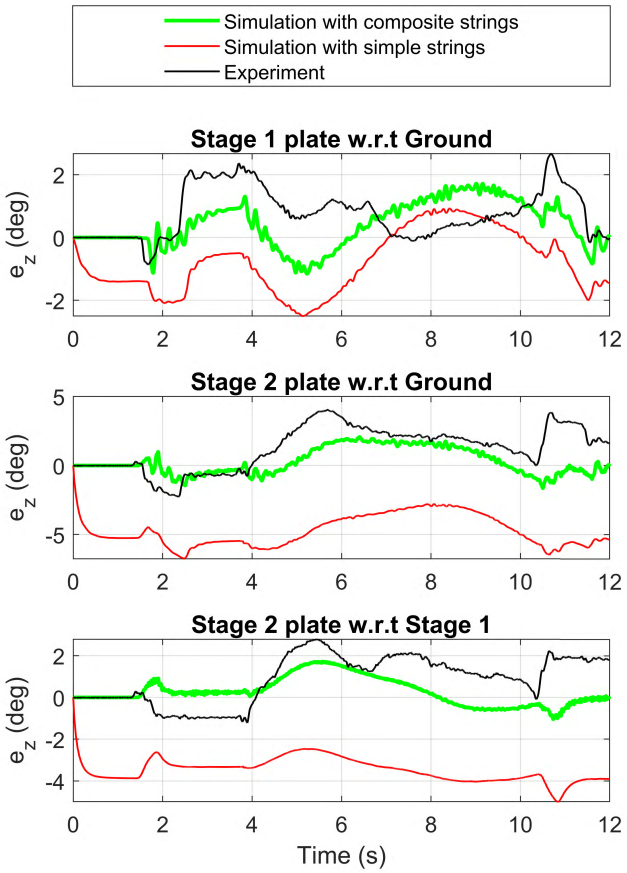

FIGURE 8. Z-axis Euler angle of the plates for the real-world experiment, simulation with composite and simulation with simple strings.

V. CONCLUSIONS

Compared to traditional rigid structures, tensegrities have multiple advantages, which make them suitable for robotic and aerospace applications. These advantages include low tensegrity to payload mass ratio, scalability from small to large sizes, increased shock absorption capability and etc. Due to their topology and configuration, tensegrity robots might be brought into motion by adjusting or shifting their equilibrium state, instead of "fighting" against it. This means that tensegrity robots can also be energy efficient. Thanks to these advantages, tensegrity robots might become valid alternatives to traditional industrial robots in the future. One of the goals of the manuscript was to prove that tensegrity structures are practically realizable. Accurate models of tensegrity robots are required in order to design and control them. Damping effects can not be ignored, but need to be incorporated into tensegrity dynamics. Similarly, utilization of less number of actuators is desirable and practical. For example, it would help to reduce the inertia of the tensegrity structure. Therefore, dynamics of tensegrity structures with simple strings connecting multiple nodes needs to be derived.

In this paper, the dynamics of tensegrity structures was modified to include the damping forces and simple strings connecting several nodes. A tensegrity robot was built in

order to test the accuracy of the dynamic formulation. Motion capture system was constructed from aluminum frames and OptiTrack cameras in order to measure the motion of the tensegrity robot during experiments. The correctness of the resultant dynamic equations was assessed by comparing the real trajectories of tensegrity structure with the simulated ones. It was shown that with damping forces on the strings the system equations closely capture the real-world dynamics. However, there are still open and unsolved problems related to tensegrity robots, e.g. optimal control and sensing of tensegrity structures are challenging tasks. Our dynamics formulation of stacked tensegrity structures is useful for the design of their control systems. Therefore, our next objective will be nonlinear model based control of tensegrity robots.

REFERENCES

[1] R. E. Skelton and M. C. de Oliveira, *Tensegrity Systems*, vol. 1. Springer, 2009.

[2] J. Y. Zhang and M. Ohsaki, "Stability conditions for tensegrity structures," *Int. J. Solids Struct.*, vol. 44, nos. 11–12, pp. 3875–3886, 2007.

[3] R. Connelly and M. Terrell, "Globally rigid symmetric tensegrities," *Struct. Topology*, no. 21, pp. 59–78, 1996.

[4] R. Connelly, "Rigidity and energy," *Invent. Math.*, vol. 66, no. 1, pp. 11–33, Feb. 1982.

[5] S. Guest, "The stiffness of prestressed frameworks: A unifying approach," *Int. J. Solids Struct.*, vol. 43, nos. 3–4, pp. 842–854, 2006.

[6] H. C. Tran and J. Lee, "Form-finding of tensegrity structures with multiple states of self-stress," *Acta Mechanica*, vol. 222, no. 1, p. 131, Aug. 2011.

[7] Y. Li, X.-Q. Feng, Y.-P. Cao, and H. Gao, "A Monte Carlo form-finding method for large scale regular and irregular tensegrity structures," *Int. J. Solids Struct.*, vol. 47, nos. 14–15, pp. 1888–1898, 2010.

[8] L. Zhang, B. Maurin, and R. Motro, "Form-finding of nonregular tensegrity systems," *J. Struct. Eng.*, vol. 132, no. 9, pp. 1435–1440, 2006.

[9] M. Yamamoto, B. Gan, K. Fujita, and J. Kurokawa, "A genetic algorithm based form-finding for tensegrity structure," *Procedia Eng.*, vol. 14, pp. 2949–2956, Jan. 2011.

[10] K. Koohestani, "Form-finding of tensegrity structures via genetic algorithm," *Int. J. Solids Struct.*, vol. 49, no. 5, pp. 739–747, 2012.

[11] M. Pagitz and J. M. Tur, "Finite element based form-finding algorithm for tensegrity structures," *Int. J. Solids Struct.*, vol. 46, no. 17, pp. 3235–3240, 2009.

[12] G. G. Estrada, H.-J. Bungartz, and C. Mohrdieck, "Numerical form-finding of tensegrity structures," *Int. J. Solids Struct.*, vol. 43, no. 22, pp. 6855–6868, 2006.

[13] J. Rieffel, F. Valero-Cuevas, and H. Lipson, "Automated discovery and optimization of large irregular tensegrity structures," *Comput. Struct.*, vol. 87, nos. 5–6, pp. 368–379, 2009.

[14] S. H. Juan and J. M. M. Tur, "Tensegrity frameworks: Static analysis review," *Mech. Mach. Theory*, vol. 43, no. 7, pp. 859–881, Jul. 2008.

[15] C. Sultan, "Tensegrity: 60 years of art, science, and engineering," *Adv. Appl. Mech.*, vol. 43, pp. 69–145, Jan. 2009.

[16] R. Motro, S. Najari, and P. Jouanna, "Static and dynamic analysis of tensegrity systems," in *Shell and Spatial Structures: Computational Aspects* (Lecture Notes in Engineering), G. De Roeck, A. S. Quiroga, M. Van Laethem, and E. Backx, Eds. Heidelberg, Germany: Springer, 1987, pp. 270–279.

[17] S. Pellegrino, "Analysis of prestressed mechanisms," *Int. J. Solids Struct.*, vol. 26, no. 12, pp. 1329–1350, 1990.

[18] I. J. Oppenheim and W. O. Williams, "Geometric effects in an elastic tensegrity structure," *J. Elasticity Phys. Sci. Solids*, vol. 59, nos. 1–3, pp. 51–65, Jun. 2000.

[19] N. Kanchanasaratool and D. Williamson, "Modelling and control of class NSP tensegrity structures," *Int. J. Control*, vol. 75, no. 2, pp. 123–139, 2002.

[20] C. Sultan, "Modeling, design, and control of tensegrity structures with applications," Ph.D. dissertation, School Aeronaut. Astronaut., Purdue Univ., West Lafayette, IN, USA, 1999.

[21] H. Murakami, "Static and dynamic analyses of tensegrity structures. Part 1. Nonlinear equations of motion," *Int. J. Solids Struct.*, vol. 38, no. 20, pp. 3599–3613, 2001.

[22] H. Murakami, "Static and dynamic analyses of tensegrity structures. Part II. Quasi-static analysis," *Int. J. Solids Struct.*, vol. 38, no. 20, pp. 3615–3629, 2001.

[23] H. Murakami and Y. Nishimura, "Static and dynamic characterization of regular truncated icosahedral and dodecahedral tensegrity modules," *Int. J. Solids Struct.*, vol. 38, nos. 50–51, pp. 9359–9381, 2001.

[24] J. M. M. Tur and S. H. Juan, "Tensegrity frameworks: Dynamic analysis review and open problems," *Mechanism Mach. Theory*, vol. 44, no. 1, pp. 1–18, 2009.

[25] J. Aldrich, R. E. Skelton, and K. Kreutz-Delgado, "Control synthesis for a class of light and agile robotic tensegrity structures," in *Proc. Amer. Control Conf.*, vol. 6, Jun. 2003, pp. 5245–5251.

[26] C. Paul, F. J. Valero-Cuevas, and H. Lipson, "Design and control of tensegrity robots for locomotion," *IEEE Trans. Robot.*, vol. 22, no. 5, pp. 944–957, Oct. 2006.

[27] W. L. Chan, D. Arbelaez, F. Bossens, and R. E. Skelton, "Active vibration control of a three-stage tensegrity structure," *Proc. SPIE*, vol. 5386, pp. 340–347, Jul. 2004.

[28] N. B. H. Ali and I. F. C. Smith, "Dynamic behavior and vibration control of a tensegrity structure," *Int. J. Solids Struct.*, vol. 47, no. 9, pp. 1285–1296, 2010.

[29] R. Skelton, "Dynamics and control of tensegrity systems," in *IUTAM Symposium on Vibration Control of Nonlinear Mechanisms and Structures*, H. Ulbrich and W. Günthner, Eds. Dordrecht, The Netherlands: Springer, 2005, pp. 309–318.

[30] R. Skelton, "Efficient dynamic models of tensegrity systems," *Model., Signal Process., Control Smart Struct.*, vol. 7286, Apr. 2009, Art. no. 72860P.

[31] R. E. Skelton, *Efficient Models of Multi-Body Dynamics*. Hoboken, NJ, USA: Wiley, 2010.

[32] J. Cheong and R. E. Skelton, "Nonminimal dynamics of general class k tensegrity systems," *Int. J. Struct. Stability Dyn.*, vol. 15, no. 2, 2015, Art. no. 1450042.

[33] H. G. Tanner and K. J. Kyriakopoulos, "Mobile manipulator modeling with Kane's approach," *Robotica*, vol. 19, no. 6, pp. 675–690, 2001.

[34] M. H. Korayem and A. M. Shafei, "A new approach for dynamic modeling of n-viscoelastic-link robotic manipulators mounted on a mobile base," *Nonlinear Dyn.*, vol. 79, no. 4, pp. 2767–2786, Mar. 2015.

[35] J. Liu and R. Liu, "Dynamic modeling of dual-arm cooperating manipulators based on Udwadia–Kalaba equation," *Adv. Mech. Eng.*, vol. 8, no. 7, pp. 1–10, 2016.

[36] G. Carpentieri and R. E. Skelton, "On the dynamics of tensegrity bridges," *J. Aerosp. Eng. Mech.*, vol. 1, no. 1, pp. 48–62, 2017.

[37] S. K. Saha and W. O. Schiehlen, "Recursive kinematics and dynamics for parallel structured closed-loop multibody systems," *Mech. Struct. Mach.*, vol. 29, no. 2, pp. 143–175, 2001.

[38] J. Naudet, D. Lefeber, F. Daerden, and Z. Terze, "Forward dynamics of open-loop multibody mechanisms using an efficient recursive algorithm based on canonical momenta," *Multibody Syst. Dyn.*, vol. 10, no. 1, pp. 45–59, Aug. 2003.

DENIS FADEYEV received the B.S. degree in robotics and mechatronics from Nazarbayev University, Astana, Kazakhstan, in 2016, where he is currently pursuing the master's degree in robotics and as a Research Assistant with the Advanced Robotics and Mechatronics Laboratory (ARMS). His research interests include tensegrity structure design, optimal control, and underactuated robotics.

ALTAY ZHAKATAYEV (M'15) received the B.S. degree in aerospace engineering from Texas A&M University, College Station, TX, USA, in 2010, and the M.S. degree in mechanical engineering from University College London, London, UK, in 2012. Since 2012, he has been with the Advanced Robotics and Mechatronics Systems (ARMS) Laboratory, Nazarbayev University, Astana, Kazakhstan, as a Research Assistant. His research interests include optimal control and the design of variable impedance actuated robots using numerical optimization.

ASKAT KUZDEUOV received the B.S. degree in automation and control engineering from the Almaty University of Power Engineering and Telecommunication, Almaty, Kazakhstan, in 2014. He is currently pursuing the master's degree with the Department of Robotics and Mechatronics, Nazarbayev University. He was a Software Engineer with Oil & Gas Industry, from 2014 to 2017. He participated in more than 30 local and international projects. His research interests include sensor fusion, computer vision and embedded systems.

HUSEYIN ATAKAN VAROL (M'09–SM'16) received the B.S. degree in mechatronics engineering from Sabancı University, Istanbul, Turkey, in 2005, and the M.S. and Ph.D. degrees in electrical engineering from Vanderbilt University, Nashville, TN, USA, in 2007 and 2009, respectively, where he was a Postdoctoral Research Associate and a Research Assistant Professor with the Center for Intelligent Mechatronics, Department of Mechanical Engineering, from 2009 to 2011.

In 2011, he joined the Faculty of Nazarbayev University, Astana, Kazakhstan, where he currently Chairs the Department and directs the Advanced Robotics and Mechatronics Systems (ARMS) Laboratory. He has published more than 50 technical papers on related topics in international journals and conferences. His research interests include biomechatronics, variable impedance actuation, machine learning, and embedded systems.

Dr. Varol was a finalist for the KUKA Innovation Award, in 2014. He was also a recipient of the IEEE International Conference on Rehabilitation Robotics Best Paper Award, in 2009 and the IEEE Engineering in Medicine and Biology Society Outstanding Paper Award, in 2013. He serves as a Technical Editor of the IEEE/ASME TRANSACTIONS ON MECHATRONICS.